Beyond receiver functions: Passive source reverse time migration and inverse scattering of converted waves

Xuefeng Shang,[1] Maarten V. de Hoop,[2] and Robert D. van der Hilst[1]

Received 7 May 2012; revised 29 June 2012; accepted 5 July 2012; published 11 August 2012.

[1] We present a wave equation prestack depth migration to image crust and mantle structures using multi-component earthquake data recorded at dense seismograph arrays. Transmitted *P* and *S* waves recorded on the surface are back propagated using an elastic wave equation solver. The wave modes are separated after the reverse-time continuation of the wavefield from the surface, and subjected to a (cross-correlation type) imaging condition forming an inverse scattering transform. Reverse time migration (RTM) does not make assumptions about the presence or properties of interfaces – notably, it does not assume that interfaces are (locally) horizontal. With synthetic experiments, and different background models, we show that passive source RTM can reconstruct dipping and vertically offset interfaces even in the presence of complex wave phenomena (such as caustics and point diffraction) and that its performance is superior to traditional receiver function analysis, e.g., common conversion point (CCP) stacking, in complex geological environments. **Citation:** Shang, X., M. V. de Hoop, and R. D. van der Hilst (2012), Beyond receiver functions: Passive source reverse time migration and inverse scattering of converted waves, *Geophys. Res. Lett.*, *39*, L15308, doi:10.1029/2012GL052289.

1. Introduction

[2] Increasingly dense seismographic arrays are being deployed all over the world in attempts to constrain subsurface structures and geological processes in greater detail. Reducing the spacing between seismograph stations will, ultimately, have diminishing returns unless we can apply imaging methods that exploit the full complexity of the recorded broadband wavefields and that do not rely on simplifying – but often profoundly limiting – prior assumptions about Earth's structure.

[3] Common conversion point (CCP) stacking techniques are now routinely applied in the receiver function workflow to image interfaces in the crust and mantle beneath the stations [e.g., *Dueker and Sheehan*, 1997; *Gilbert et al.*, 2003; *Zhu*, 2000]. For smoothly varying structures this can produce good results [e.g., *Zhai and Levander*, 2011], but the horizontal interface assumption in CCP stacking prevents the accurate imaging of geologically complex structures, such as dipping and laterally discontinuous interfaces (e.g., strong interface topography, steep faults, steps in Moho). Moreover, stacking data from individual stations cannot adequately suppress scattering or diffraction "artifacts" [e.g., *Chen et al.*, 2005; *Rondenay*, 2009; *Sheehan et al.*, 2000].

[4] With access to data from dense arrays we can avoid stacking in the spatial domain, e.g., over a presumed horizontal interface, and propagate scattered energy back to the subsurface point where scattering occurs. Reverse time migration (RTM) improves image quality remarkably. Migration is based on the single scattering approximation and does not distinguish between refraction and reflection. Its application to refraction data, however, is more recent than its application to reflection data [see *Levander et al.*, 2005].

[5] There are different types of seismic imaging method. We consider reverse time migration [*Baysal et al.*, 1983; *McMechan*, 1983; *Whitmore*, 1983] and the category of approaches known under the collective names of Kirchhoff migration [*Bleistein et al.*, 2001] or generalized Radon transform inversion. For example, *Beylkin* [1985] and *Stolk and de Hoop* [2002] analyze inverse scattering using asymptotic methods and *Op't Root et al.* [2012] use the full-wave equation. Applications to global seismology, with waveform data from earthquakes, which (relative to active source exploration) introduces complications due to uncertainties in hypocenter location and source signature, can be found in *Rondenay et al.* [2001], *Poppeliers and Pavlis* [2003], and *Chen et al.* [2005]. Ray theory yields high frequency solutions of the wave equation and essentially is applicable in sufficiently smooth background models. Solving the full wave equation leads to robust solutions, which admit background models of limited regularity.

[6] *Brytik et al.* [2012] developed a comprehensive theory for RTM-based (elastic) inverse scattering with converted waves in anisotropic media. Building on that analysis we present here a wave equation method for the migration of converted waves to image crust and mantle structures using teleseismic array data. Here, we use a bilinear imaging operator acting on the data, which is essentially a cross-correlation operator of all receiver pairs. Passive source RTM of converted waves differs fundamentally from single station receiver function (RF) analysis and also in several important ways from more traditional RF migration by, for instance, *Chen et al.* [2005]. Firstly, it concerns reverse-time continuation, in which the raw data from individual earthquakes are back propagated, whereas *Chen et al.* [2005] uses CCP stacked RFs, which degrades spatial resolution because of the implicit 1D assumption in RF construction that the interfaces are (locally) horizontal. Moreover, it solves the elastic wave

[1]Department of Earth, Atmospheric, and Planetary Sciences, Massachusetts Institute of Technology, Cambridge, Massachusetts, USA.
[2]Department of Mathematics, Purdue University, West Lafayette, Indiana, USA.

Corresponding author: X. Shang, Department of Earth, Atmospheric, and Planetary Sciences, Massachusetts Institute of Technology, 77 Massachusetts Ave., Cambridge, MA 02139, USA. (xfshang@mit.edu)

0094-8276/12/2012GL052289

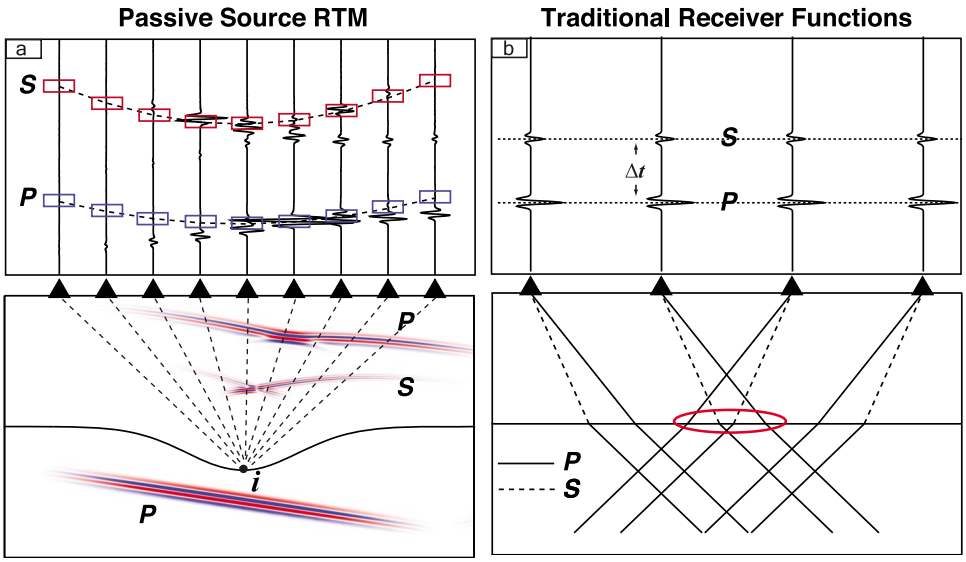

Figure 1. Schematic illustration of (a) passive-source reverse time migration and (b) common conversion point (CCP) stacking of traditional receiver functions. (a) (bottom) *P* waves impinging on a contrast produces direct *P* and converted *S* waves, which can be recorded at an array of seismograph stations at the surface (black triangles). (top) *P* and *S* energy due to scattering at, say, point *i* arrives at different times (blue and red boxes, respectively). In inverse sense, the location point *i* can be reconstructed by optimization of the correlation between the backprojected *P* and *S* wavefields. (b) (bottom) In traditional receiver functions, the *P*-*SV* conversion is assumed to occur at an interface that is (locally) horizontal. (top) The travel time difference Δt between transmitted *P* and converted *S* is a measure of interface depth, and data redundancy is obtained by stacking over common conversion points (CCP), shown as a red oval.

equations explicitly and accounts for wave phenomena such as the formation of caustics underneath the array.

2. Methodology

[7] Teleseismic *P* (or *S*) waves impinging on an interface from below can convert to other modes (e.g., *P*-to-*S* or *S*-to-*P*), which then propagate with different wave speeds to seismographs at the Earth's surface (Figure 1). With assumed wave propagation speeds and angles of incidence, traditional receiver functions simply convert the arrival time difference between transmitted and converted phases as measured at a single station down to the depth where the conversion occurs (Figure 1b), and signal-to-noise is enhanced by stacking over data with common conversion points. As is illustrated in Figure 1b, for single station RF analysis the points where refraction (e.g., *P*-*P*) and mode conversion (e.g., *P*-*S*) occur are not the same, which introduces the need to assume that – at least locally (that is, within the first Fresnel zone of the incident wave) – the interface is horizontal. In contrast, RTM exploits the entire wave field, as sampled by a dense array, to locate the points where scattering (including mode conversion) occurs (Figure 1a). Noise suppression in RTM occurs through the continuity property of the underlying inverse scattering transform on the one hand and through stacking over different sources (or events) on the other hand. The resolution can be expressed in terms of the Rayleigh diffraction limit (e.g., $\lambda/4$, λ is the incident wave wavelength).

[8] Snapshots of the wave field can be reconstructed by back propagation of the recorded array data. Due to the difference in *P* and *S* wavespeed, the relevant parts of the transmitted and converted wave fronts were in the same location only at the time of conversion. While strictly correct only in the absence of multiple scattering, this observation was used in developing the basic "imaging condition" [e.g., *Claerbout*, 1971] in exploration seismology. The conversion time (and the corresponding location of the point where conversion occurred) can be found by applying the imaging condition (here, a cross-correlation function between different wave modes).

[9] There are three main steps in teleseismic, passive source RTM. Firstly, for each earthquake, using reverse-time continuation, the snapshots of the elastic wave field are reconstructed from the recorded multicomponent array data. Secondly for each snapshot *P* and *S* constituents are separated by polarization decomposition (detailed later). Finally the imaging condition, derived from a cross-correlation between *P* and *S* wave constituents, is applied. The final image is then obtained by summation of the images from individual events.

[10] A major challenge for passive source RTM is the uncertainty in source signature and the fact that all sources are different. For *P* (*S*) wave incidence we estimate the source signature from the vertical (radial) component array data by multichannel analysis, e.g., multichannel cross correlation (MCCC) and principle component analysis (PCA) [*Rondenay and Fischer*, 2003; *VanDecar and Crosson*, 1990]. The elastic Green's functions are then estimated by deconvolution of the source signature from all three components, and the wave field is reconstructed by reverse-time continuation from the surface boundary data [e.g., *McMechan*, 1983]. Here we solve the elastic wave equation in the time domain using a staggered grid finite difference propagator [*Virieux*, 1986].

[11] In 3-D (isotropic elastic media), for each time step, the reconstructed displacement wavefield $\mathbf{u}_r$ can be decoupled

into *P*, *SV* and *SH* components by projection operators Q^* [*Brytik et al.*, 2011]:

$$u_{r,\mathrm{P}} = Q^*_{\mathrm{P}}\,\mathbf{u}_r \quad u_{r,\mathrm{SV}} = Q^*_{\mathrm{SV}}\,\mathbf{u}_r \quad \text{and} \quad u_{r,\mathrm{SH}} = Q^*_{\mathrm{SH}}\,\mathbf{u}_r, \tag{1}$$

which are defined as

$$\begin{aligned} Q^*_{\mathrm{P}} &= (-\Delta)^{-1/2}\frac{1}{i}\left(\frac{\partial}{\partial x_1}\ \ \frac{\partial}{\partial x_2}\ \ \frac{\partial}{\partial x_3}\right)\\ Q^*_{\mathrm{SV}} &= (-\Delta)^{-1/2}(-\Delta)^{-1/2}\left(\frac{\partial^2}{\partial x_1\partial x_3}\ \ \frac{\partial^2}{\partial x_2\partial x_3}\ \ -\frac{\partial^2}{\partial x_1^2}-\frac{\partial^2}{\partial x_2^2}\right)\\ Q^*_{\mathrm{SH}} &= (-\Delta')^{-1/2}\frac{1}{i}\left(-\frac{\partial}{\partial x_2}\ \ \frac{\partial}{\partial x_1}\ \ 0\right) \end{aligned} \tag{2}$$

Here, Δ is the Laplacian operator, Δ' is $\partial^2/\partial x_1^2 + \partial^2/\partial x_2^2$, and i is the imaginary unit. In 2-D these operators degenerate to:

$$\begin{aligned} Q^*_{\mathrm{P}} &= (-\Delta)^{-1/2}\frac{1}{i}\left(\frac{\partial}{\partial x_1}\ \ \frac{\partial}{\partial x_2}\right)\\ Q^*_{\mathrm{S}} &= (-\Delta')^{-1/2}\frac{1}{i}\left(-\frac{\partial}{\partial x_2}\ \ \frac{\partial}{\partial x_1}\right) \end{aligned} \tag{3}$$

After decoupling of *P* and *SV* components, the imaging condition for *P* wave incidence from a single source is applied [*Brytik et al.*, 2012]:

$$I(\mathbf{x}) = \int_0^T \left\{ \left(\frac{1}{i}\partial_t u_{r,\mathrm{p}}(\mathbf{x},t)\right)\left(\frac{1}{i}\partial_t u_{r,\mathrm{sv}}(\mathbf{x},t)\right) + \left(\frac{1}{i}\nabla\right)u_{r,\mathrm{p}}(\mathbf{x},t)\cdot\left(\frac{1}{i}\beta(\mathbf{x})(-\Delta)^{-1/2}\partial_t\nabla\right)u_{r,\mathrm{sv}}(\mathbf{x},t)\right\}dt \tag{4}$$

where T is the total recorded time, and $\beta(\mathbf{x})$ is *S* wave velocity. For *S* wave incidence, one can exchange $u_{r,\mathrm{p}}$ with $u_{r,\mathrm{sv}}$ and replace $\beta(\mathbf{x})$ by $\alpha(\mathbf{x})$ (*P* wave velocity). At sufficiently high frequencies the operator $(-\Delta)^{-1/2}\,\partial_t$ can be approximated (in the asymptotic limit) as $\beta(\mathbf{x})$ − or $\alpha(\mathbf{x})$ for *S* wave incidence.

[12] The transmission (reflection) coefficient $\mathbf{T_{ps}}$ ($\mathbf{R_{ps}}$) is an odd function of *P* wave incidence angle [*Aki and Richards*, 2002; *Balch and Erdemir*, 1994]. In absence of elaborate corrections for radiation patterns [see *Brytik et al.*, 2012], at least we need to correct for the sign of converted *SV* waves in order to constructively sum all partial images. We determine the sign by evaluating the Poynting vector [e.g., *Červený*, 2001; *Dickens and Winbow*, 2011] to find the incidence angle of *P* wave and transmission angle of converted *SV* wave. The sign of *SV* waves is then reversed, if necessary.

3. Numerical Examples

[13] We demonstrate the performance of converted wave RTM with numerical experiments, using synthetic data generated by a fourth order finite difference scheme. We also investigate the effect of background models on image quality and compare the performances of RTM with CCP stacks of RFs. Two models with lateral heterogeneities are employed to generate synthetic data: a lens-kink model and a layer-kink model (Figures 2c and 2d). Both models contain a discontinuous interface. In the lens-kink model a Gaussian low velocity lens is used to investigate effects of wave phenomena caused by a low velocity anomaly in the crust. Caustics can be observed in the data recorded at the surface (two components of the particle velocity) (Figure 2a, inset). Interior (explosive) point sources are placed at the bottom of the models (Figures 2c and 2d) and injected as *P* arrivals. We use a total of 22 events, but the contribution of individual sources is also illustrated. The central frequency of the source function is 2 Hz. The spacing between receivers (at the surface) is 300 m, which is smaller than the "spatial" Nyquist frequency and avoids "spatial" aliasing.

[14] To assess the effect of background model, we use two types of model for the inversion step (that is, the back propagation): a 1-D model with a linear increase of wave speed with depth (Figure 3a) and a 2-D smooth model with (smooth) spatial variations in wave speed that resemble the actual structures (Figure 3d). We note that the latter could be obtained, for instance, through tomography. Comparing the RTM imaging results for the lens-kink model (Figures 3b and 3e), the kink structure is, as expected, better recovered if we use the 2-D background model. Absence of the low velocity lens in the background model introduces artificial topography on the horizontal layer between 20∼40 km horizontal distance (Figure 3e), and inclusion of the lens (Figure 3d, inset) yields near perfect recovery (Figure 3e, inset). In the layer-kink model, the 2D smooth model improves the reconstruction of the vertical structure (Figure 3f) and the flat interface below the kink. The amplitude along this flat interface is not balanced (e.g., amplitude decrease can be observed for x > 50 km range) due to illumination effects; this common phenomenon can be corrected in angle domain [e.g., *Wu et al.*, 2004] but that is not done here. A partial image from one earthquake (Figure 3f, inset) suggests that the main structures can be revealed by only a few events as long as they provide good illumination.

[15] In Figure 4 we compare converted wave RTM with CCP stacking results. The models used to generate the synthetic wavefields are the same as in Figure 3 except the edges of the kink discontinuity are smoothed to suppress the corner diffraction that would otherwise overwhelm the CCP stacks even more. Three localized plane waves (plane waves tapered by a Gaussian window) with different position and incident angles are used as incident waves (Figures 4a and 4d). For this comparison, we use the same 1-D background model for CCP stacking and RTM. Even for this relatively simple model, the wave field appears to be too complicated for CCP stacking to reconstruct the input model (Figures 4b and 4e). Indeed, the horizontal interfaces can barely be discerned among the image artifacts, and the vertical structure is not recovered at all. In contrast, despite the complexity of the wavefield, the RTM images reveal clearly the interfaces, even with data from only three sources.

4. Discussion

[16] Linearized imaging methods, either ray-based or wave equation based, are sensitive to the background model. We demonstrate here that a background model with lateral heterogeneity can greatly improve the image quality, especially near vertical structures. A smooth background model can be estimated from geological models, from travel time or surface wave tomography – either in active or passive (e.g., ambient noise) studies, or by wave equation (WE) reflection tomography [*Burdick et al.*, 2012]. Indeed, in the future we aim to combine passive source RTM and WE reflection

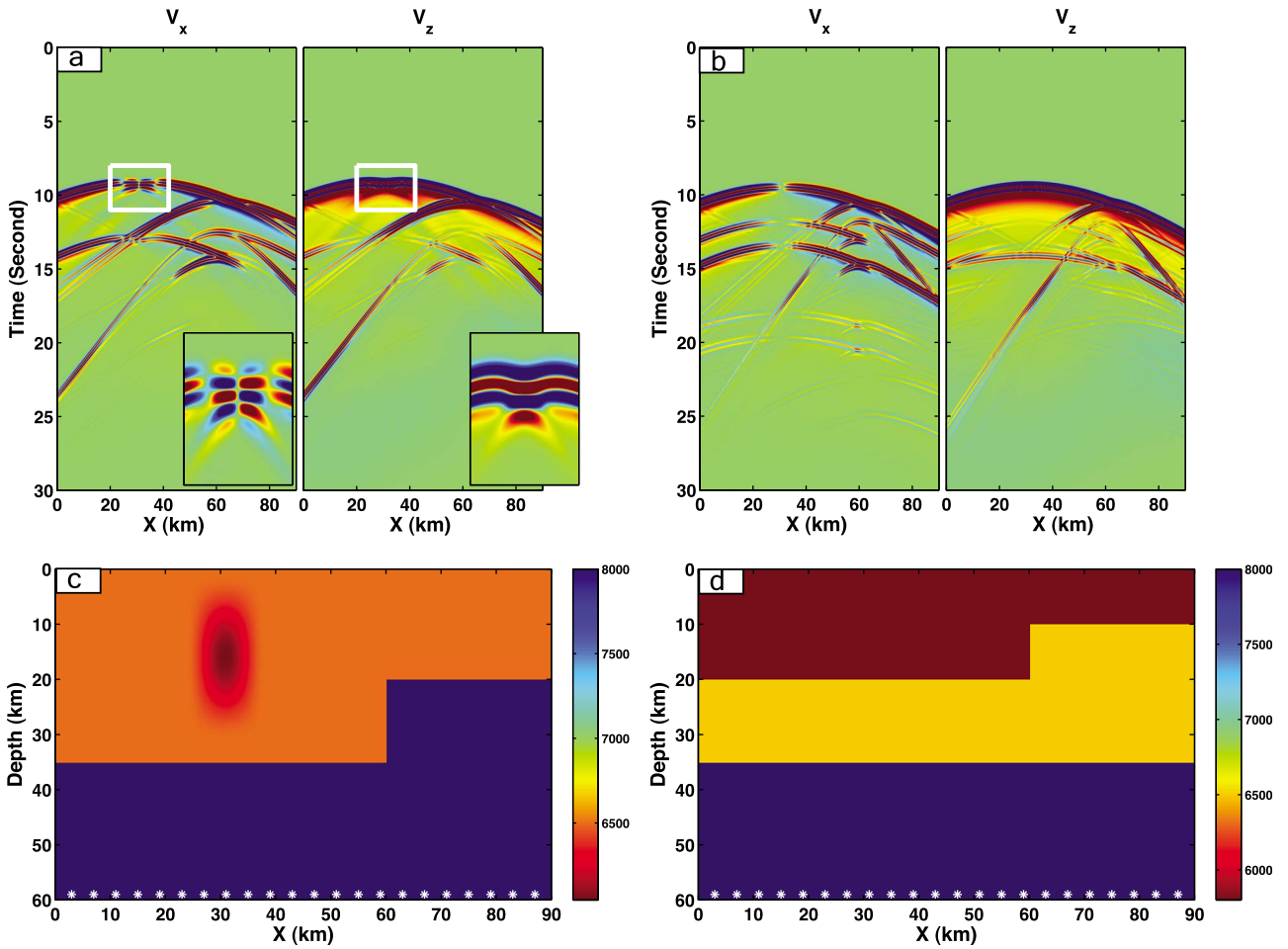

Figure 2. (a, b) Synthetic data computed for two test models – (c) a lens-kink model and (d) a layer-kink model – with v_x and v_z the horizontal and vertical components, respectively, of particle velocity. The dimension of the models is 90 km by 60 km. Receivers are at the surface and up to 22 (explosive) sources are located at the bottom of the models, shown as white stars in Figures 2c and 2d. The source central frequency is 2 Hz, and a Ricker wavelet is chosen as the source time function. In the lens-kink model, a 7% low velocity Gaussian lens forms a crustal low velocity anomaly; the caustics produced by this lens are visible in the inset of Figure 2a. Corresponding *S* and mass density models are obtained through scaling of the *P* models shown here.

tomography in an explicit (non-linear) joint inversion of teleseismic wavefields for wavespeed and interface location.

[17] With the simple models used here, the kinked interface violates the flat layer assumption in CCP stacking and the low velocity lens causes the formation of caustics that cannot be accounted for with CCP stacking. The diffraction artifacts in the CCP stacking image can be suppressed somewhat if more events are included, but breakdown of (translational) symmetry assumptions cannot be avoided. In contrast, RTM – a wave equation method based on an artifact-free imaging condition – accounts for wavefield complexity and effectively migrates corner diffraction energy back to the proper position in the final image (Figures 4c and 4f). Another indication of the promise of passive source RTM is that only a few earthquakes with good illumination coverage and high signal-to-noise ratio are sufficient, even in geological environments that render CCP stacking ineffective. Given the irregular distribution of naturally occurring earthquakes, our method can improve seismic imaging in large areas, provided, of course, that data from dense seismograph arrays are available.

[18] In our demonstration of the concept and promise of passive source RTM we suppressed several practical challenges. Firstly, RTM has stringent sampling requirements. The sampling theorem suggests that the spatial interval Δx, in principle, should be less than $(\lambda_a)_{min}/2$, where $(\lambda_a)_{min}$ is the minimum horizontal apparent wavelength for a given depth. For a typical teleseismic study, with frequencies around or above 1 Hz, a station interval of 5 km should be sufficient (see *Chen et al.* [2005] for details). In the real acquisition, irregular and sparse (aliased) sampled data can introduce significant "noise" in RTM. Such problems can be partially mitigated by interpolation in frequency-wavenumber [*Spitz*, 1991; *Zwartjes and Sacchi*, 2007] or curvelet domain [*Naghizadeh and Sacchi*, 2010]. Secondly, the effect of limited illumination needs to be compensated in passive source RTM. In our experiments, the 22 point sources at the bottom provide near full illumination coverage. In real data, the incident angle of teleseismic wave is constrained in a narrow range (~15°–40°) due to the sparsity and irregularity of the earthquake distribution. This means that geological structures can only be partially imaged. The illumination

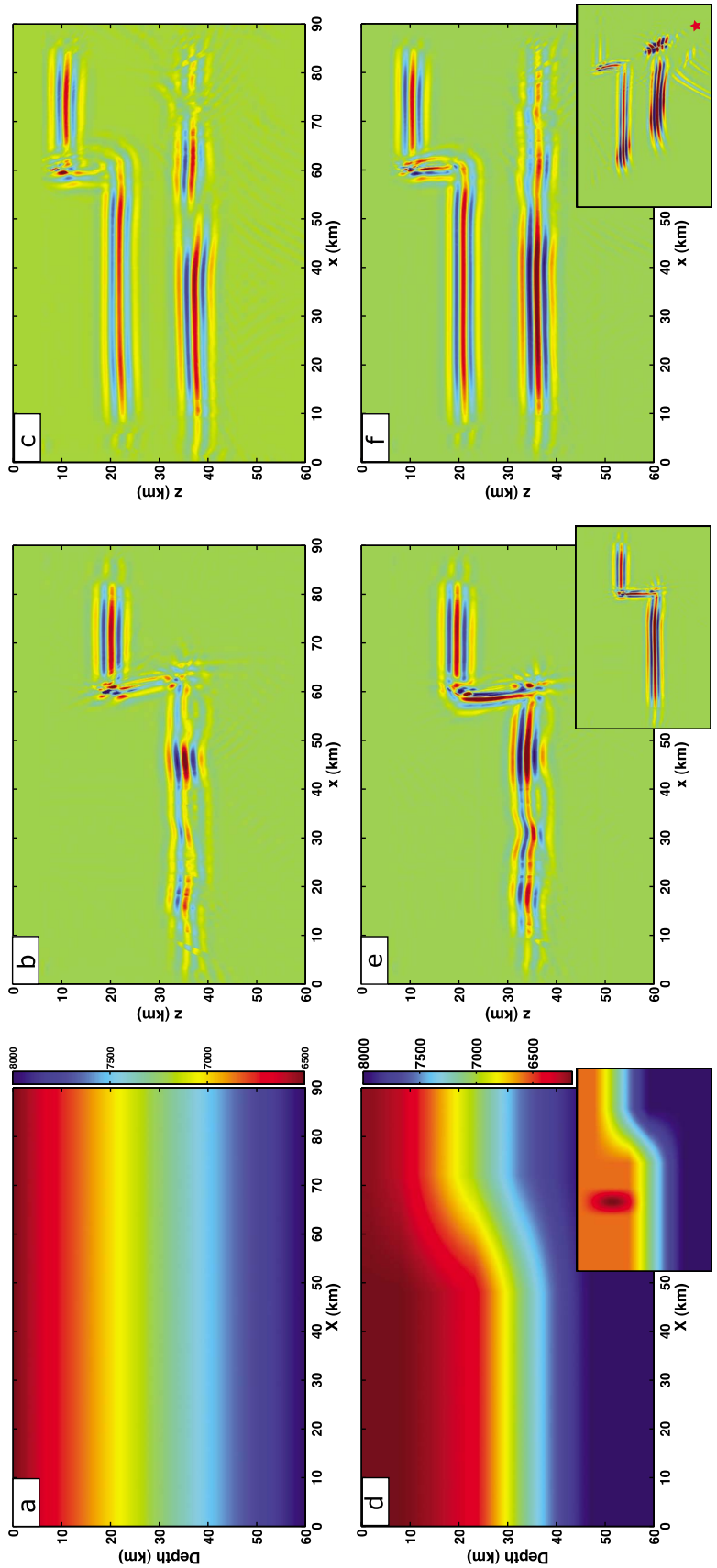

Figure 3. Background models and converted wave RTM imaging results. (a) Gradual increase of wavespeed with depth. (b, c) Recovery of the lens-kink model (data shown in Figure 2a) and layer-kink model (data in Figure 2b) using the 1-D background model shown in Figure 3a. (d) Smooth 2-D background (inset: with low velocity lens). (e) Recovery of the lens-kink model with the 2-D background model (inset: recovery using 2-D model that includes the low velocity lens). (f) Recovery of the layer-kink model with the 2-D background model (inset: partial image obtained with data from a single source, red star).

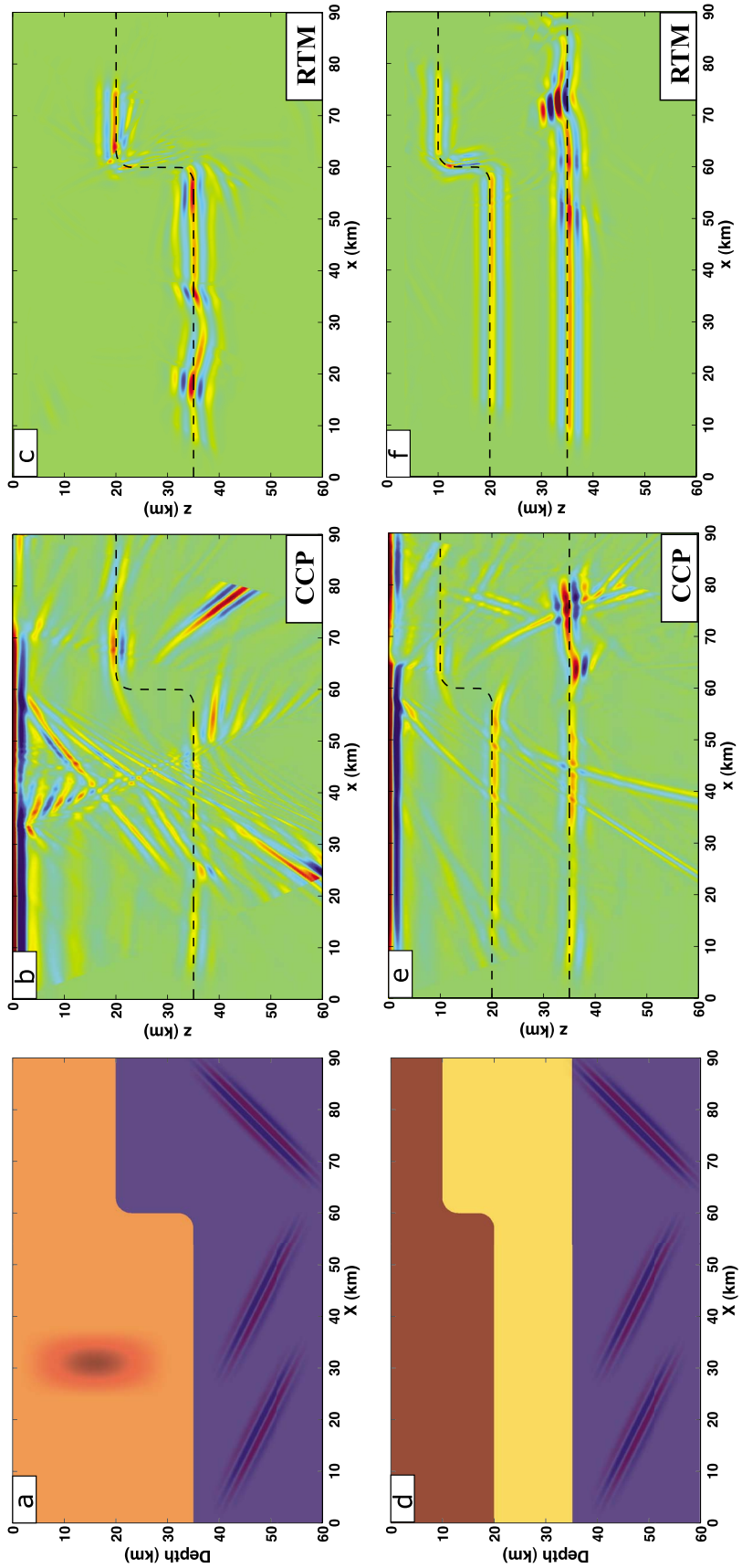

Figure 4. Comparison between CCP stacking and RTM. (a) Lens-kink model. Three localized *P* plane waves are used as incident sources to generate synthetic data. The localized plane waves with different incident angles are shown in the bottom layer. (b) CCP stacking results using 1D linearly increased model. (c) RTM result based on the same 1D model as in Figure 4b. (d) Layer-kink model. The same localized *P* plane waves as of Figure 4a are used for the generation of synthetic data. (e) CCP stacking results using 1D linearly increased model. (f) RTM result based on the same 1D model as in Figure 4e. The dashed lines in Figures 4b, 4c, 4e, and 4f show the interfaces in true models (Figures 4a and 4d).

(aperture) effect can be corrected by computing the (diagonal of) normal operator and its approximate inverse [e.g., *de Hoop et al.*, 2009]. Another problem is the presence of multiples, for instance the reverberation in shallow sedimentary layers. Certain techniques from exploration seismology can to some extent suppress the multiples [e.g., *Berkhout and Verschuur*, 1997]. These challenges are not unique to RTM, however, and thus beyond the scope of this paper.

5. Conclusions

[19] We present a method for subsurface imaging with multi-component data from dense seismograph arrays that does not rely on simplifying (e.g., 1-D) assumptions about the geometry of the geological structures of interest. The array data are backward propagated by solving the elastic wave equation directly. After polarization separation, a modified cross correlation imaging condition between *P* and *S* wave constitutes is applied to obtain an inverse scattering transform. From synthetic experiments, it is evident that for complex geological structures the new method is superior to the traditional CCP receiver function stacking, provided that data from dense seismograph arrays are available. At present, few arrays are suitable for application of teleseismic RTM without substantial preprocessing (including interpolation), but in view of the trend to deploy increasingly dense arrays we expect that passive source RTM will become feasible – and even routine – in the near future.

[20] **Acknowledgments.** We thank Alan Levander and an anonymous reviewer for their valuable comments.

[21] The Editor thanks Alan Levander and Satish Singh for assisting in the evaluation of this paper.

References

Aki, K., and P. G. Richards (2002), *Quantitative Seismology*, University Sci. Sausalito, Calif.

Balch, A., and C. Erdemir (1994), Sign change correction for prestack migration of P-S converted wave reflections, *Geophys. Prospect.*, *42*(6), 637–663, doi:10.1111/j.1365-2478.1994.tb00233.x.

Baysal, E., D. D. Kosloff, and J. W. C. Sherwood (1983), Reverse time migration, *Geophysics*, *48*(11), 1514–1524.

Berkhout, A. J., and D. J. Verschuur (1997), Estimation of multiple scattering by iterative inversion, Part I: Theoretical considerations, *Geophysics*, *62*(5), 1586–1595.

Beylkin, G. (1985), Imaging of discontinuities in the inverse scattering problem by inversion of a causal generalized Radon transform, *J. Math Phys. N. Y.*, *26*, 99–108, doi:10.1063/1.526755.

Bleistein, N., J. K. Cohen, and J. W. Stockwell (2001), *Mathematics of Multidimensional Seismic Imaging, Migration, and Inversion*, Springer, New York, doi:10.1115/1.1399683.

Brytik, V., M. V. de Hoop, H. F. Smith, and G. Uhlmann (2011), Decoupling of modes for the elastic wave equation in media of limited smoothness, *Commun. Partial Differ. Equations*, *36*(10), 1683–1693, doi:10.1080/03605302.2011.558554.

Brytik, V., M. V. de Hoop, and R. D. van der Hilst (2012), Elastic-wave inverse scattering based on reverse time migration with active and passive source reflection data, in *Inside Out: Inverse Problems*, Cambridge Univ. Press, Cambridge, U. K., in press.

Burdick, S., M. de Hoop, S. Wang, and R. van der Hilst (2012), Teleseismic wave-equation reflection tomography using free surface reflected phases, *Geophys. J. Int.*, in press.

Červený, V. (2001), *Seismic Ray Theory*, Cambridge Univ. Press, Cambridge, U. K., doi:10.1017/CBO9780511529399.

Chen, L., L. Wen, and T. Zheng (2005), A wave equation migration method for receiver function imaging: 1. Theory, *J. Geophys. Res.*, *110*, B11309, doi:10.1029/2005JB003665.

Claerbout, J. F. (1971), Toward a unified theory of reflector mapping, *Geophysics*, *36*, 467–481.

de Hoop, M., H. Smith, G. Uhlmann, and R. Van der Hilst (2009), Seismic imaging with the generalized Radon transform: A curvelet transform perspective, *Inverse Probl.*, *25*, 025005, doi:10.1088/0266-5611/25/2/025005.

Dickens, T. A., and G. A. Winbow (2011), RTM angle gathers using Poynting vectors, *SEG Expanded Abstr.*, *30*, 3109.

Dueker, K. G., and A. F. Sheehan (1997), Mantle discontinuity structure from midpoint stacks of converted P to S waves across the Yellowstone hotspot track, *J. Geophys. Res.*, *102*, 8313–8327, doi:10.1029/96JB03857.

Gilbert, H. J., A. F. Sheehan, K. G. Dueker, and P. Molnar (2003), Receiver functions in the western United States, with implications for upper mantle structure and dynamics, *J. Geophys. Res.*, *108*(B5), 2229, doi:10.1029/2001JB001194.

Levander, A., F. Niu, and W. W. Symes (2005), Imaging teleseismic P to S scattered waves using the Kirchhoff integral, in *Seismic Earth: Array Analysis of Broadband Seismograms*, *Geophys. Monogr. Ser.*, vol. 157, edited by A. Levander and G. Nolet, pp. 149–169, AGU, Washington, D. C., doi:10.1029/157GM10.

McMechan, G. A. (1983), Migration by extrapolation of time-dependent boundary values, *Geophys. Prospect.*, *31*(3), 413–420, doi:10.1111/j.1365-2478.1983.tb01060.x.

Naghizadeh, M., and M. D. Sacchi (2010), Beyond alias hierarchical scale curvelet interpolation of regularly and irregularly sampled seismic data, *Geophysics*, *75*(6), WB189–WB202.

Op't Root, T. J. P. M., C. C. Stolk, and M. V. de Hoop (2012), Linearized inverse scattering based on reverse time migration, *J. Math. Pures Appl.*, *98*, 211–238.

Poppeliers, C., and G. L. Pavlis (2003), Three-dimensional, prestack, plane wave migration of teleseismic P-to-S converted phases: 1. Theory, *J. Geophys. Res.*, *108*(B2), 2112, doi:10.1029/2001JB000216.

Rondenay, S. (2009), Upper mantle imaging with array recordings of converted and scattered teleseismic waves, *Surv. Geophys.*, *30*(4–5), 377–405, doi:10.1007/s10712-009-9071-5.

Rondenay, S., and K. M. Fischer (2003), Constraints on localized core-mantle boundary structure from multichannel, broadband SKS coda analysis, *J. Geophys. Res.*, *108*(B11), 2537, doi:10.1029/2003JB002518.

Rondenay, S., M. G. Bostock, and J. Shragge (2001), Multiparameter two-dimensional inversion of scattered teleseismic body waves: 3. Application to the Cascadia 1993 data set, *J. Geophys. Res.*, *106*(B12), 30,795–30,807, doi:10.1029/2000JB000039.

Sheehan, A. F., P. M. Shearer, H. J. Gilbert, and K. G. Dueker (2000), Seismic migration processing of P-SV converted phases for mantle discontinuity structure beneath the Snake River Plain, western United States, *J. Geophys. Res.*, *105*(B8), 19,055–19,065, doi:10.1029/2000JB900112.

Spitz, S. (1991), Seismic trace interpolation in the F-X domain, *Geophysics*, *56*(6), 785–794.

Stolk, C. C., and M. V. de Hoop (2002), Microlocal analysis of seismic inverse scattering in anisotropic elastic media, *Commun. Pure Appl. Math.*, *55*(3), 261–301, doi:10.1002/cpa.10019.

VanDecar, J., and R. Crosson (1990), Determination of teleseismic relative phase arrival times using multi-channel cross-correlation and least squares, *Bull. Seismol. Soc. Am.*, *80*(1), 150–159.

Virieux, J. (1986), P-SV wave propagation in heterogeneous media: Velocity-stress finite-difference method, *Geophysics*, *51*(4), 889–901.

Whitmore, N. D. (1983), Iterative depth migration by backward time propagation, *SEG Expanded Abstr.*, *2*(1), 382, doi:10.1190/1.1893867.

Wu, R. S., M. Luo, S. Chen, and X. B. Xie (2004), Acquisition aperture correction in angle domain and true amplitude imaging for wave equation migration, *SEG Expanded Abstr.*, *23*(1), 937, doi:10.1190/1.1845319.

Zhai, Y., and A. Levander (2011), Receiver function imaging in strongly laterally heterogeneous crust: Synthetic modeling of BOLIVAR data, *Earth Sci.*, *24*(1), 45–54, doi:10.1007/s11589-011-0768-4.

Zhu, L. (2000), Crustal structure across the San Andreas Fault, Southern California from teleseismic converted waves, *Earth Planet. Sci. Lett.*, *179*(1), 183–190, doi:10.1016/S0012-821X(00)00101-1.

Zwartjes, P., and M. Sacchi (2007), Fourier reconstruction of nonuniformly sampled, aliased seismic data, *Geophysics*, *72*(1), V21–V32.